Thermo X https://doi.org/10.70401/tx.2026.0032

Supplementary information

Atomic-level engineering thermal transport anisotropy in C24 monolayers for directional heat spreading

Qikun Tian1, Ruyi Li, Hongkai Zhang, Enbo Zhang, Xiong Zheng, Huimin Wang, Zhenzhen Qin, Guangzhao Qin

Table S1 Lattice constants of qTP and qHP C_{24} monolayers

materials	Lattice parameters (Å)		
	DFT	NEP	NEP-Reference [1]
2D qTP	a = 6.089, b = 6.089	a = 6.105, b = 6.105	a = 6.103, b = 6.103
2D qHP	a = 11.472, b = 6.168	a = 11.479, b = 6.178	a = 11.500, b = 6.180

Table S2 Hyperparameters for the NEP model.

parameter	value	parameter	value
r_c^R	7 Å	r_c^A	4 Å
n_{max}^R	10	n_{max}^A	8
N_{bas}^R	10	N_{bas}^A	8
l_{max}^{3b}	4	l_{max}^{4b}	2
N_{neu}	30	λ_1	0.044
λ_2	0.044	λ_e	1
λ_f	1	λ_v	0.5
N_{bat}	1000	N_{pop}	50
N_{gen}	2×10^5		

Table S3 Thermal conductivity κ (W m^{-1} K^{-1}) of various 2D materials at 300 K.

phase	Method	Functional Type	Energy cutoff	κ_x	κ_y
qTP C_{24}	HNEMD (This work)	PBEsol	800 eV	234	234
	HNEMD [2]	PBE	650 eV	272	272
qHP C_{24}	HNEMD (This work)	PBEsol	800 eV	130	216
	HNEMD [2]	PBE	650 eV	233	341
qHP C_{60}	HNEMD [3]	PBE	650 eV	102	137
graphene	DFT [4]	PBEsol	110 Ry	3552	3552
	DFT [4]	PBE	110 Ry	3850	3850
black phosphorene	DFT [5]	PBEsol	700 eV	5.91	1.06
	DFT [5]	PBE	700 eV	14.89	2.42

Table S4 Elastic constants C_{ij} (N/m) of monolayer carbon allotropes.

phase	Method	Functional Type	C_{11}	C_{22}	C_{12}	C_{66}
qTP C_{24}	DFT (This work)	PBEsol	248.6	248.6	-11.9	80.8
	DFT [2]	PBE	251.3	251.3	−4.4	79.9
	NEP (This work)	PBEsol	236.1	236.1	-11.1	84.3
	NEP [2]	PBE	248.8	248.8	−15.8	81.6
qHP C_{24}	DFT (This work)	PBEsol	225.2	274.0	21.3	105.0
	DFT [2]	PBE	225.1	275.7	23.6	106.0
	NEP (This work)	PBEsol	216.7	266.2	26.0	108.5
	NEP [2]	PBE	236.5	295.4	24.4	110.3
qTP2 C_{60}	DFT [6]	PBEsol	149.9	148.7	22.9	53.4
qHP C_{60}	DFT [6]	PBEsol	150.8	186.8	22.5	60.6
graphene	DFT [7]	PBE	351.4	351.4	61.6	144.9

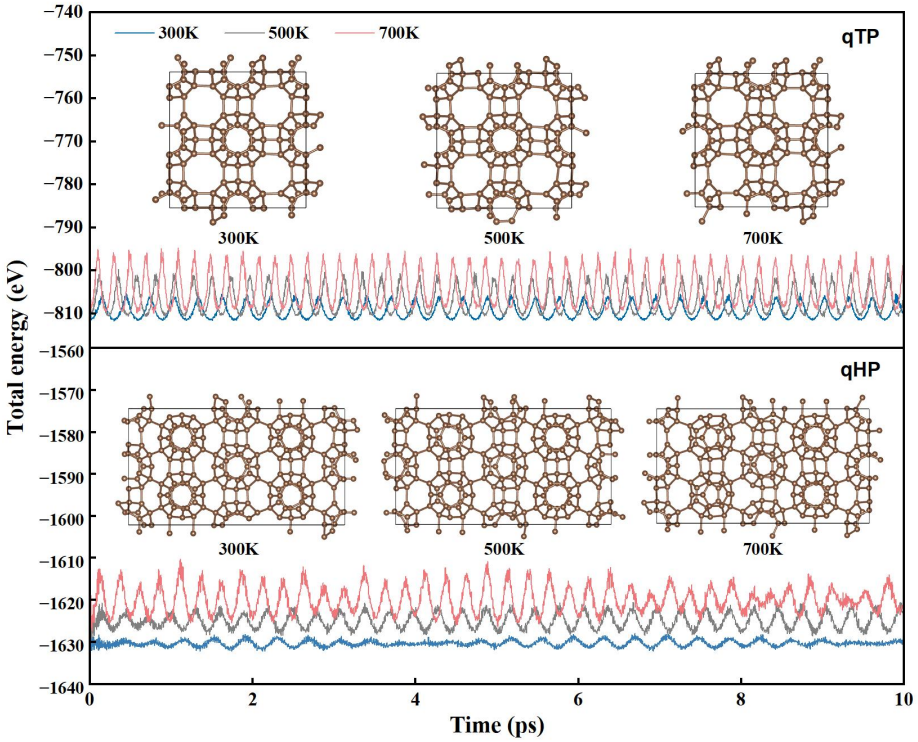

Figure S1 Simulation of total energy fluctuations in the qTP and qHP phases via AIMD, conducted for 10 ps with a 1 fs time step at 300, 500, and 700 K. The subfigures show the corresponding atomic structures at the end of each simulation.

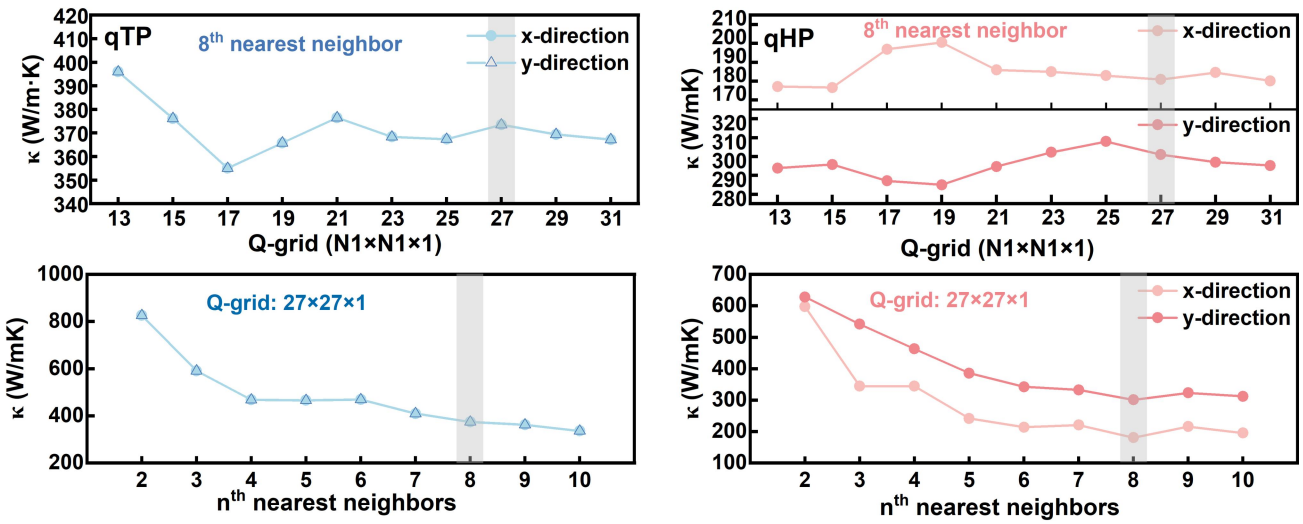

Figure S2 Convergence of the thermal conductivity with the nearest neighbor and the Q-grid. The value within the gray box represents the converged result.

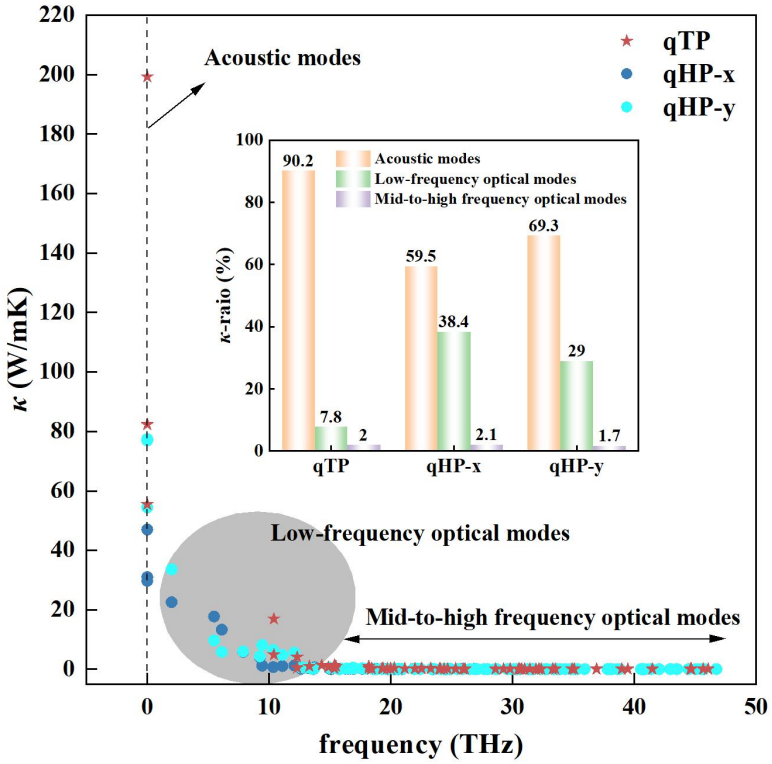

Figure S3 Frequency-resolved contributions of individual phonon modes to the lattice thermal conductivity of qTP and qHP C_{24} monolayers. The inset shows the relative contributions from acoustic, low-frequency optical, and mid-to-high-frequency optical modes.

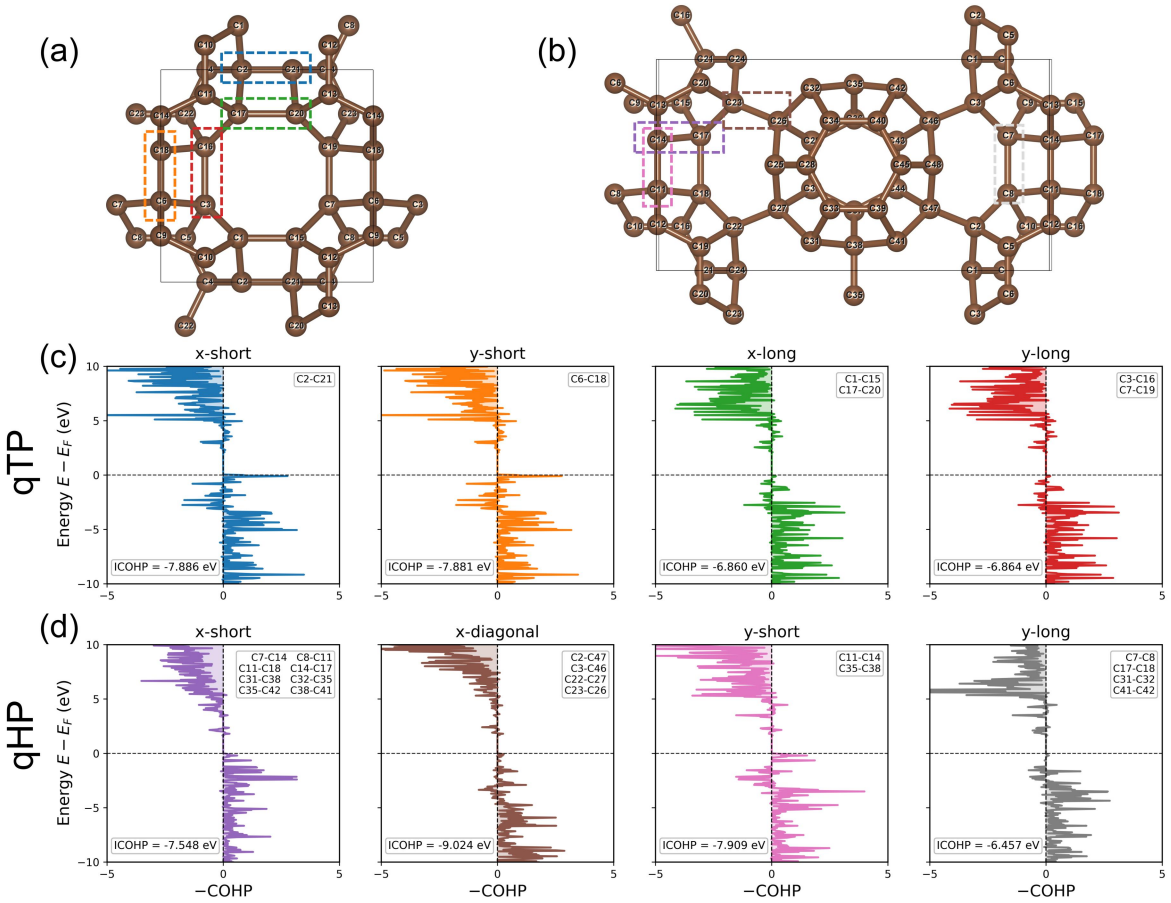

Figure S4 Atomic bonding configurations and COHP analysis of qTP and qHP C_{24} monolayers. (a) Top view of the qTP C_{24} structure, with the representative inter-cage C–C bonds along the x- and y-directions highlighted by dashed boxes. (b) Top view of the qHP C_{24} structure, showing the characteristic x-short, x-diagonal, y-short, and y-long inter-cage bonding configurations. (c) Energy-resolved −COHP curves for the x-short, y-short, x-long, and y-long bonds of qTP C_{24}. (d) Energy-resolved −COHP curves for the x-short, x-diagonal, y-short, and y-long bonds of qHP C_{24}. The corresponding C–C atom pairs are labeled in the upper-right corner of each panel, while the ICOHP values at the Fermi level are given in the lower-left corner. For bond classes containing multiple symmetry-equivalent C–C pairs, the displayed −COHP curves and ICOHP values are averaged over the listed bonds.

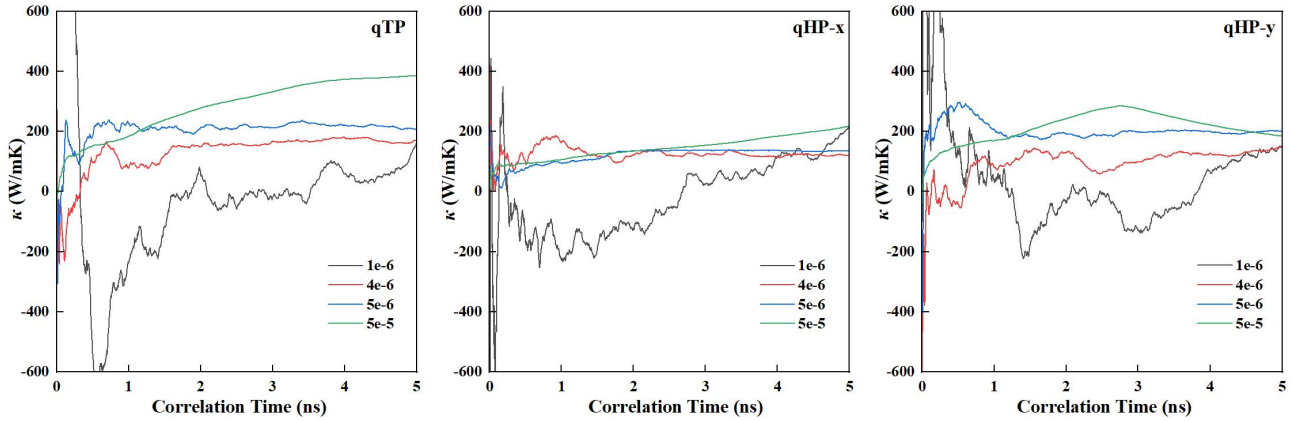

Figure S5 Convergence of the thermal conductivity with correlation time under different external driving forces for qTP and qHP in the x- and y-directions.

References:

[1] J. Wu and B. Peng, Smallest [5,6]Fullerene as Building Blocks for 2D Networks with Superior Stability and Enhanced Photocatalytic Performance, J. Am. Chem. Soc. **147**, 1749 (2025).

[2] Q. Li, H. Dong, P. Ying, and Z. Fan, Anisotropic and isotropic elasticity and thermal transport in monolayer C24 networks from machine-learning molecular dynamics, International Journal of Heat and Mass Transfer **260**, 128505 (2026).

[3] H. Dong, C. Cao, P. Ying, Z. Fan, P. Qian, and Y. Su, Anisotropic and high thermal conductivity in monolayer quasi-hexagonal fullerene: A comparative study against bulk phase fullerene, Int. J. Heat Mass Transfer **206**, 123943 (2023).

[4] A. Taheri, S. Pisana, and C. V. Singh, Importance of quadratic dispersion in acoustic flexural phonons for thermal transport of two-dimensional materials, Phys. Rev. B **103**, 235426 (2021).

[5] F. Zhang, X. Zheng, H. Wang, L. Ding, and G. Qin, Anisotropy of thermal transport in phosphorene: A comparative first-principles study using different exchange–correlation functionals, Mater. Adv. **3**, 5108 (2022).

[6] B. Peng, Stability and strength of monolayer polymeric C_{60}, Nano Lett. **23**, 652 (2023).

[7] B. Liu, T. Gao, P. Liao, Y. Wen, M. Yao, S. Shi, and W. Zhang, Metallic VS_2 /graphene heterostructure as an ultra-high rate and high-specific capacity anode material for li/na-ion batteries, Phys. Chem. Chem. Phys. **23**, 18784 (2021).